World Academy of Science, Engineering and Technology
International Journal of Aerospace and Mechanical Engineering
Vol:14, No:9, 2020

A FE-Based Scheme for Computing Wave Interaction with Nonlinear Damage and Generation of Harmonics in Layered Composite Structures

R.K. Apalowo, D. Chronopoulos

Abstract—A Finite Element (FE) based scheme is presented for quantifying guided wave interaction with Localised Nonlinear Structural Damage (LNSD) within structures of arbitrary layering and geometric complexity. The through-thickness mode-shape of the structure is obtained through a wave and finite element method. This is applied in a time domain FE simulation in order to generate time harmonic excitation for a specific wave mode. Interaction of the wave with LNSD within the system is computed through an element activation and deactivation iteration. The scheme is validated against experimental measurements and a WFE-FE methodology for calculating wave interaction with damage. Case studies for guided wave interaction with crack and delamination are presented to verify the robustness of the proposed method in classifying and identifying damage.

Keywords—Layered Structures, nonlinear ultrasound, wave interaction with nonlinear damage, wave finite element, finite element.

I. Introduction

LINEAR ultrasonic wave techniques have been widely developed for monitoring the condition and residual life estimation of in-service composite structures. However, these techniques are generally limited to relatively large defects but much less sensitive to micro and nonlinear defects. Therefore there is a need to develop nonlinear acousto-ultrasonic technique which will detect and evaluate nonlinear incipient defects in composite structures efficiently and reliably.

Finite Element (FE) based nonlinear wave interaction has been studied numerically using unilateral contact laws. These laws are available in commercial FE packages and have been used to study nonlinear wave interaction with delamination [1], breathing [2] and buried [3] cracks. Despite the reported attempts to capture wave interaction with localised structural nonlinearities and damage, there is currently limited computational scheme for predicting these quantities in composite structures of arbitrary layering and geometric complexity.

The Wave and Finite Element (WFE) method was introduced in [4], [5] in order to facilitate the post-processing of eigenproblem solutions. The WFE has recently found applications in predicting the vibroacoustic and dynamic performance of composite panels and shells [6], [7], [8] , with complex periodic structures [9], [10], [11] having been investigated. The variability of vibroacoustic transmission through layered structures [12], [13], [14], as well as structural identification [15] have also been considered.

The main contribution of the work presented in this chapter is the development of a generic WFE based computational scheme for computing wave interaction with localised nonlinear structural damage (LNSD) in arbitrarily layered composite structures. It is also aimed at establishing the computed harmonic wave interaction coefficients as a damage mode identification tool.

The principal contribution of this work is the development of a generic WFE based computational scheme for computing wave interaction with localised nonlinear structural damage (LNSD) in arbitrarily layered composite structures. It is also aimed at establishing the computed harmonic wave interaction coefficients as a damage mode identification tool. The paper is organised as follows: Section II presents the overview of the problem statement. Sections III and IV respectively present the nonlinear damage modelling and the FE wave interaction simulation. In Section V, experimental and numerical case studies are presented for validating the exhibited scheme. Conclusions are drawn in Section VI.

II. Statement of the Problem

Wave propagation is considered in the x direction of an arbitrarily layered composite structure, periodic in the x direction. In general case, plane strain condition is assumed in the z direction and the structure can exhibit structural nonlinearity, such as nonlinear/clapping damage as shown in Fig. 1.

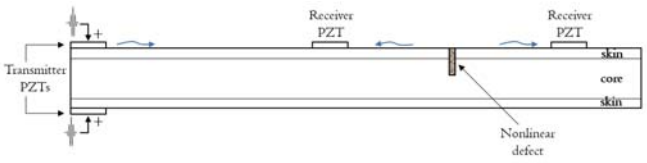

Fig. 1 Arbitrarily layered composite structure containing structural defect exhibiting nonlinear mechanical behaviour. Imposed wave signal is received after interaction with the nonlinear defect

The wave propagation constants at each periodic cross-section of the structure are obtained through the WFE scheme, as described in [15]. The WFE-computed mode shape of a specific wave at the left extreme cross-section of the plate is piezoelectrically generated, as a voltage tone burst signal

R.K. Apalowo and D. Chronopoulos are with the Composites Research Group & Institute for Aerospace Technology, The University of Nottingham, NG7 2RD, UK.

R.K. Apalowo is with the Mechanical Engineering Department, Federal University of Technology, Akure, Nigeria (e-mail: kayodeapalowo@gmail.com).

of the wave, and imposed on the extreme cross-section as shown in Fig. 1. Quantification of the wave signal interaction with the nonlinear damage is hereby considered.

III. Nonlinear Structural Damage Modelling

A. Harmonics Generation through Contact Acoustic nonlinearity

Contact acoustic nonlinearity (CAN) is generated when a propagating wave interacts with nonlinear/micro damage within a structural medium. This leads to a clapping mechanism of the damage being activated during the interaction. The clapping mechanism, during which the damage opens and closes alternatively, leads to the generation of sub and higher harmonics of the wave. Hence, wave interaction with nonlinear damage is expected to generate interaction scattering coefficients not only at fundamental frequency but also at sub and higher harmonic frequencies. This feature is highly essential in accessing nonlinearity within structural systems. As will be demonstrated in later sections, it is also essential for damage detection and identification.

B. Element Birth/Death Criterion for Modelling Clapping Mechanism of Nonlinear Damage

The clapping mechanism of a nonlinear structural damage involves an asynchronous opening or closing of the damage as a wave travels through it. The damage closes during the compressional phase of the wave, and opens during the tensile phase as shown in Fig. 2. In CAN, compressive stress strengthens the contact between interface surfaces of the defect while tensile stress weakens it. Hence, the compressional phase of the wave penetrates the defect and closes it while the tensile part opens it.

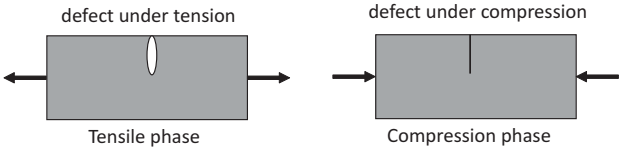

Fig. 2 Acoustic mechanism in a contact-type damage: the damage opens under tension and closes when in compression

The clapping mechanism of the damage is implemented in an element birth/death criterion. In the criterion, elements within the damage zone are deactivated (damage opens) when their cumulative strains are positive (i.e. when undergoing tension) and reactivated (damage closes) when negative (i.e. when undergoing compression). It should be noted that when elements are deactivated, they are not removed or deleted from the structural model, but rather made insignificant in the model. Hence, during this stage, the material stiffness of the deactivated finite elements is reduced by a severe reduction factor [16]. This leads to an updated stiffness matrix in order to accommodate reduction in stiffness properties of the medium. As structural matrices (mass, stiffness or damping) are an assemblage of constituent elements matrices, the stiffness matrix of the affected elements is updated as

$$\boldsymbol{K}_u^e = \beta \boldsymbol{K} \tag{1}$$

where $\boldsymbol{K}$ is the original stiffness matrix of the elements when active (alive), $\boldsymbol{K}_u^e$ is the updated stiffness matrix of the elements when deactivated (dead) and β is the stiffness reduction factor (equals 10^{-6} by default or a user defined value, typically $\ll 1$). On the other hand, the mass matrix of the deactivated elements are set to zero to remove their effect from the entire model.

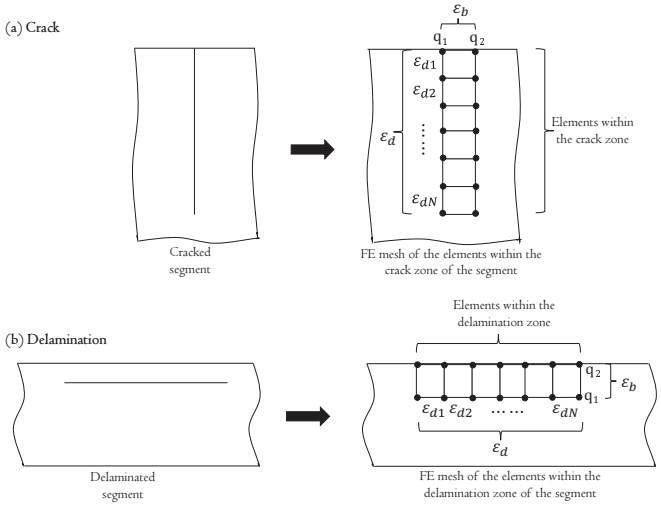

Fig. 3 Configuration of the element birth/death criterion for damage clapping mechanism: (a) Crack (b) Delamination. (Not to scale)

As earlier stated, deactivation of the elements within the damage zone depends on the cumulative strain value of the elements. The cumulative strain of the damage zone elements, as illustrated in Fig. 3, are determined as

$$\begin{aligned} \varepsilon_d &= \sum_{n=1}^{N} \varepsilon_{dn} \\ \varepsilon_b &= q_2 - q_1 \end{aligned} \tag{2}$$

with all strain values measured along the axis of wave propagation.

The iterative procedure of the elements birth/death criterion for nonlinear wave interaction modelling is summarised in the pseudocode presented in Algorithm 1.

The algorithm presents the routine through which the elements within the damage zone are systematically made active or inactive during the nonlinear transient analysis. After each solution step, the cumulative strains $(\varepsilon_d, \varepsilon_b)$ of the damage zone elements are calculated (2). The elements are made inactive if the magnitudes of the strains are positive (i.e. under tension) or active if the strain values are negative (i.e. under compression). This iteration is repeated for every load step of the analysis.

IV. Finite Element Wave Interaction Modelling

Each supported wavemode (obtained through the WFE scheme) w with $\mathrm{w} \in [1 \cdots \mathrm{W}]$, at a specified angular

Algorithm 1 Iterative procedure of the element birth/death criterion for damage clapping mechanism

1: Build the model, apply load and constraints and determine solution parameters
2: $i \leftarrow 1$ (first solution step)
3: Solve the model for solution step i
4: Determine ε_d and ε_b
5: **if** $\varepsilon_d < 0 \cap \varepsilon_b < 0$ **then**
6: Reactivate the damage zone elements if presently deactivated
7: **else**
8: Deactivate the damage zone elements if presently active
9: **end if**
10: **if** $i \leq m$ (where m equals number of solution steps) **then**
11: $i \leftarrow i + 1$ (next solution step)
12: Go to step 3
13: **else**
14: End of iteration
15: **end if**

frequency, can be grouped into displacement and force components as

$$\begin{aligned}
\mathbf{\Phi}_q^{\text{inc}} &= \left[\begin{array}{cccc} \phi_{q,1}^{\text{inc}} & \phi_{q,2}^{\text{inc}} & \cdots & \phi_{q,W}^{\text{inc}} \end{array}\right]_{[j\times W]} \\
\mathbf{\Phi}_f^{\text{inc}} &= \left[\begin{array}{cccc} \phi_{f,1}^{\text{inc}} & \phi_{f,2}^{\text{inc}} & \cdots & \phi_{f,W}^{\text{inc}} \end{array}\right]_{[j\times W]} \\
\mathbf{\Phi}_q^{\text{ref}} &= \left[\begin{array}{cccc} \phi_{q,1}^{\text{ref}} & \phi_{q,2}^{\text{ref}} & \cdots & \phi_{q,W}^{\text{ref}} \end{array}\right]_{[j\times W]} \\
\mathbf{\Phi}_f^{\text{ref}} &= \left[\begin{array}{cccc} \phi_{f,1}^{\text{ref}} & \phi_{f,2}^{\text{ref}} & \cdots & \phi_{f,W}^{\text{ref}} \end{array}\right]_{[j\times W]}
\end{aligned} \tag{3}$$

The displacement eigenvectors of each positive going elastic wave $\boldsymbol{\phi}_{q,\text{w}}^{\text{inc}}$ can be further grouped as

$$\boldsymbol{\phi}_{q,\text{w}}^{\text{inc}} = \left\{\begin{array}{cccccc} \boldsymbol{q}_{1,x} & \boldsymbol{q}_{1,y} & \boldsymbol{q}_{2,x} & \boldsymbol{q}_{2,y} & \cdots & \boldsymbol{q}_{r,x} \quad \boldsymbol{q}_{r,y} \end{array}\right\}^{\intercal} \tag{4}$$

with $\boldsymbol{q}_{r,x}$ and $\boldsymbol{q}_{r,y}$ the in-plane (x-axis) and the out-of-plane (y-axis) displacement components of node r where $r \in [1 \cdots R]$. R is the number of nodes along a periodic cross-section of the structural waveguide. Hence, the displacement vectors of each propagating wave, in the in-plane $\boldsymbol{\phi}_{q,\text{w}x}^{\text{inc}}$ and out-of-plane $\boldsymbol{\phi}_{q,\text{w}y}^{\text{inc}}$ directions, can be extracted from (3) and (4).

In order to generate ultrasonic wave of a specific mode and avoid mix-mode effect, the transmitter PZTs are excited, employing the WFE computed displacement of the mode being excited, at one extreme cross-section of the waveguide. This will suppress other modes within the waveguide. The wave is excited as a time-dependent harmonic voltage boundary condition (of excitation frequency ω).

Generally, in this study, the in-plane mode $\boldsymbol{\phi}_{q,\text{w}x}^{\text{inc}}$ is applied to generate a longitudinal wave motion. The excitation signal is a 20 V peak-to-peak Hanning windowed toneburst consisting of five cycles at center frequency of $f_0 = 100$ kHz. The time dependent harmonic voltage (with $\omega = 2\pi f_0$) is given as

$$V(t) = \begin{cases} \phi_{q,\text{w}x}^{\text{inc}} \sin(\omega t) \cdot (0.5 - 0.5\cos(\frac{\omega t}{5}), & t \leq \frac{10\pi}{\omega} \\ 0, & t > \frac{10\pi}{\omega} \end{cases} \tag{5}$$

After each solution step of the transient analysis, decision is made to decide whether to deactivate or reactivate the elements within the damage zone. The decision is based on the outcome of the element birth/death criterion presented in Algorithm 1.

V. Experimental and Numerical Case Studies

The presented scheme is validated in this section through experimental, as well as numerical results.

A. Experimental validation

The computational scheme exhibited in this study is applied in a cracked plate shown in Fig. 4. The plate, which is made of aluminium (whose material properties are presented in Table I), is 1.2 m long, 0.7 m wide and 0.001 m thick. The fatigue crack is produced by machining a notch at 0.7 m from the left edge of the plate and runs transversely through the plate's width. The plate is then subjected to cyclic loading under a loading machine until a fatigue crack is developed at the notch site. A range of cracks of different widths and depths are studied. The crack widths considered are within the range of 0.5 and 5.0 of the plate thickness at depths of 25% and 50% of the plate thickness.

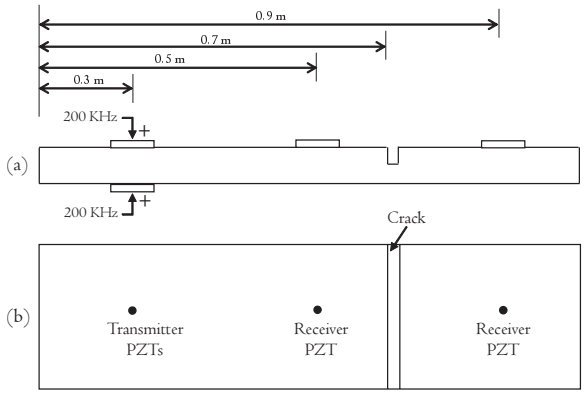

Fig. 4 Schematic representation of the cracked plate set-up: (a) front view; (b) plan view

TABLE I
Material Properties of the Materials Used for the Case Studies

	Aluminium	Mild steel	Glass fibre
ρ	2600 kg/m^3	7800 kg/m^3	1400 kg/m^3
E_x	68.95 GPa	208 GPa	45 GPa
E_y	-	-	16 GPa
E_z	-	-	16 GPa
ν_{xy}	0.3	0.3	0.28
ν_{yz}	-	-	0.4
ν_{xz}	-	-	0.28
G_{xy}	-	-	5.83 GPa
G_{yz}	-	-	5.79 GPa
G_{xz}	-	-	5.83 GPa

In order to validate the presented scheme, the results derived through the scheme are compared against those obtained through experimental measurements and those of the WFE-FE methodology presented in [17].

The test rig set-up for the experimental measurements is shown in Fig. 5. At a given frequency, there exist at least two Lamb modes propagating through an aluminium plate [18]. However, single mode excitation and monitoring make wave interaction measurement easier and more accurate without mixed-mode effect. Due to its simple and non-dispersive characteristics at low frequencies, the set-up is designed with the aim of exciting and receiving only symmetric Lamb wave mode. This is achieved by sticking two piezoelectric transducers (referred to as the transmitter PZT) on the double surface at the excitation point, with the two actuators having same coordinates as shown in Fig. 4. Exciting these two transmitter PZTs with the same input signal, symmetric mode will be generated, while the antisymmetric mode will be suppressed. Similar approach can be applied to excite only antisymmetric mode, but with the directions of the input signals in opposite sense to each other. Two additional piezoelectric transducers (referred to as the receiver PZT) are bonded on the plate at 0.5 m and 0.9 m to respectively receive the reflected and transmitted wave signals from the crack.

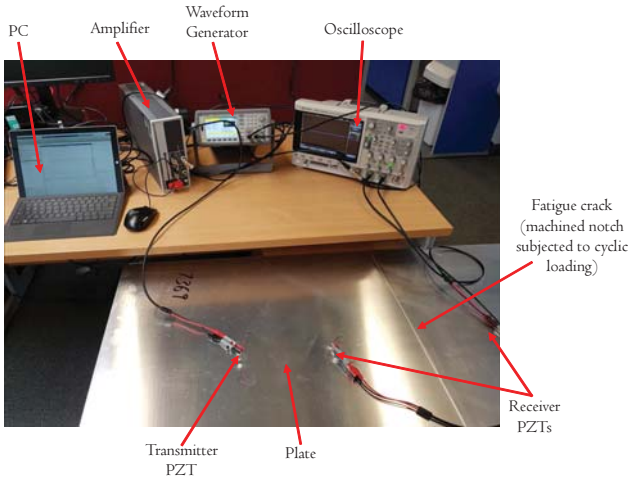

Fig. 5 Assembly of the experimental configuration

The waveform of the reflected output signal after interaction with the fatigue crack in the plate is presented in Fig. 6. The crack in this case is 0.5 mm deep and 2.5 mm wide. The output signal waveform is superimposed with that measured from the damage free (pristine) plate. It can be observed from Fig. 6 that, compared with the pristine plate waveform history, there exist a new wave packet generated in the damage plate waveform history. It therefore follows that the new signal packet is generated by an interaction of the travelling wave with the crack. Another evident difference is that the damaged plate signal has a slight phase shift and amplitude drop which can be attributed to energy leakage during generation of the new signal packet.

FFT of the measured responses is conducted to obtain the frequency spectral of the output signals. Unwanted signals

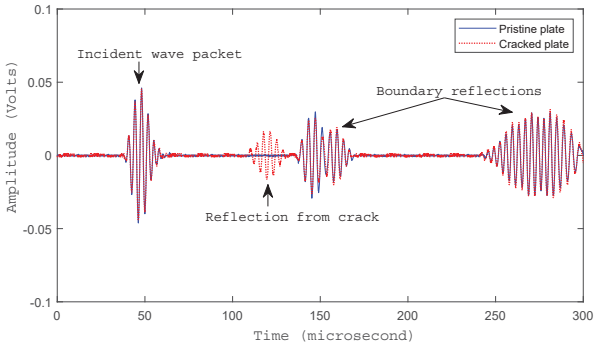

Fig. 6 Superimposed experimental time record for pristine (-) and cracked (. . .) plates. Crack is 0.5 mm deep and 2.5 mm wide

such as the edge reflections are gated out during the FFT analysis. The wave reflection coefficient is therefore calculated by dividing the frequency spectrum of the reflected signal by that of the incident signal.

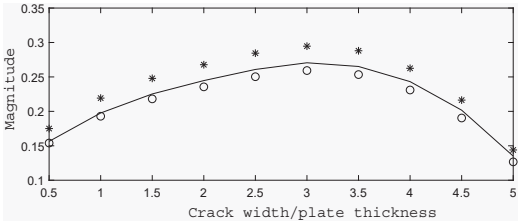

(a) 25% crack depth/plate thickness

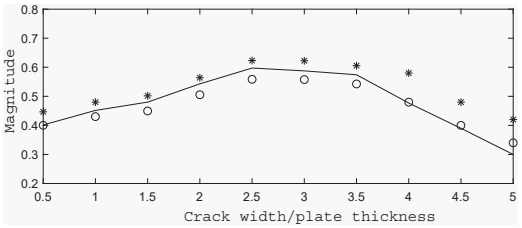

(b) 50% crack depth/plate thickness

Fig. 7 Wave reflection coefficients from the crack as a function of the crack width/plate thickness: Current scheme (o), Experimental measurements (-), WFE-FE methodology [17] (*)

The superimposed results of the presented approach, experimental measurements and WFE-FE methodology [17] are shown in Fig. 7. The results present wave reflection coefficients, at fundamental frequency, as a function of the crack width for crack depths of 25% and 50% of the plate thickness. The crack width axis is normalised to the plate thickness, so that the results may be applied equally to other thicknesses of the plate provided that the frequency-thickness of 200 kHz-mm is also maintained. The reflection coefficient magnitude in each case increases with respect to the crack width until the crack has reached a width of about 3.0 of the plate thickness. Beyond this level, the coefficient magnitude decreases with respect to the crack width until it tends towards zero value, and then increases again in a sinusoidal-like fashion.

As shown in Fig. 7, results obtained by the presented scheme agree very well with the experimental measurements

with a maximum difference of about 6%. Compared with the WFE-FE predictions, the difference rises to about 18%. This difference can be attributed to energy leakage to higher harmonics in the nonlinear analysis. It should be noted that the WFE-FE model is a linear wave interaction analysis with no leakage of energy to harmonics generation. Hence, the difference.

B. Numerical Validation

1) Description and Boundary Condition of the Model: A sandwich composite plate of thickness 2 mm and length $l_p = 1000$ mm is considered as shown in Fig. 8. The viscoelastic sandwich plate is made of a glass fibre core sandwiched between isotropic skins. The material properties of the plate's constituents are presented in Table I). The thickness of the core $h_c = 1.6$ mm while that of each skin $h_s = 0.2$ mm. Piezoelectric sensors, each of length 7 mm and thickness 0.2 mm, are bonded on the plate as shown in Fig. 8. Material properties of the piezoelectric are presented in Table II.

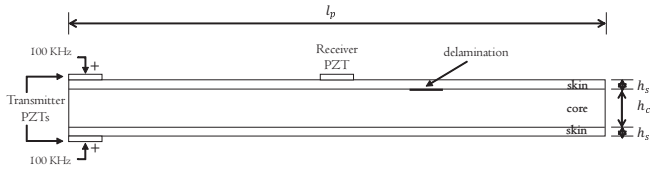

Fig. 8 FE modelling configuration for sandwich plate with a delamination

TABLE II
MATERIAL PROPERTIES OF THE PIEZOELECTRIC SENSOR

Parameter	Value	Unit
Density	$\rho = 7750$	kg/m^3
Loss tangent	$\tan\delta = 0.02$	-
Elastic flexibility	$S_{11} = S_{33} = 16.4$ $S_{22} = 18.8$ $S_{12} = S_{21} = -7.22$ $S_{13} = S_{31} = -5.74$ $S_{23} = S_{32} = -7.22$ $S_{44} = S_{55} = 47.5$ $S_{66} = 44.3$	10^{-12} m^2/N
Piezoelectric strain coefficients	$d_{21} = -1.71$ $d_{22} = 3.74$ $d_{23} = -1.71$ $d_{14} = 5.84$ $d_{35} = 5.84$	10^{-10} m/V
Electric permittivity	$\varepsilon_{11} = 2.12$ $\varepsilon_{22} = 1.75$ $\varepsilon_{33} = 2.12$	10^{-8} F/m

Interaction of guided wave with skin-core delamination is considered. Calculations are made for undamaged plate, plate with linear delamination and plate with nonlinear delamination in order to distinguish wave interaction phenomenon in each scenario of structural condition.

In order to exhibit the effect of the delamination severity on the wave interaction phenomenon, interaction coefficients are obtained as a function of the delamination widths. Delamination widths of 0.2, 0.4, 0.6, 0.8, 1.0, 1.2, 1.4 and 1.6 (all in millimetre) are considered. These correspond to 0.1 to 0.8 of the plate thickness. The delamination severity is scaled to normalise the delamination width to the plate thickness, so that the results obtained can be applied equally to other thicknesses of the plate provided that the frequency-thickness of 200 kHz-mm is satisfied.

In each case, the delamination is situated at 600 mm from the transmitter PZT, and reflection from the guided wave interaction with the delamination is received at the receiver PZT located 100 mm away from the delamination. The configuration is as shown in Fig. 8.

2) Pristine Plate: The plate in its undamaged state is first considered as a baseline for other conditions of the plate to be considered.

Fig. 9 presents the calculated time history of the signal, obtained at the receiver PZT, for the undamaged plate. As observed, there exist a single wavelet in the predicted response which suggests that the wave interact with no form of damage/discontinuities during propagation along the plate. The frequency spectrum (as shown in Fig. 10) of the wavelet also gives only the fundamental frequency component which ascertain the absence of any form of nonlinearity in the pristine plate.

3) Interaction with Linear Delamination: Guided wave interaction with linear delamination within the sandwich plate is considered in this section. As a linear analysis, the plate remains delaminated throughout the calculation window.

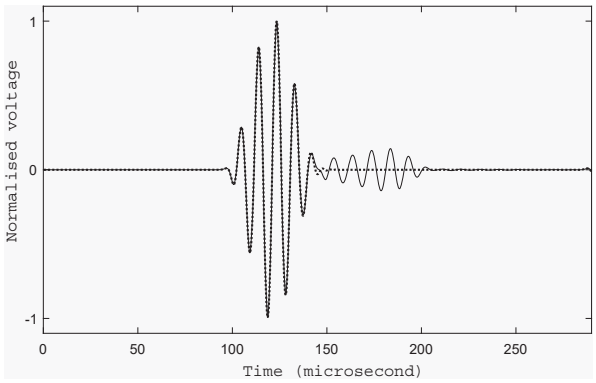

Fig. 9 Superimposed time history predictions for the pristine plate ($\cdots$) and the plate with linear delamination (-)

Fig. 9 presents the time domain response of the guided wave interaction with linear delamination within the plate superimposed with the time history obtained for the pristine plate.

The pristine plate response contains only the incident wavelet while the plate with linear delamination contains incident and reflected wavelets. The presence of the reflected wavelet is an indication of damage, in the structural waveguide, which interact with the guided wave during propagation. This establish the application of the developed scheme for damage detection.

The frequency spectrum of the incident wavelet, in the time history (Fig. 9) of the plate with linear delamination, when the reflected wavelet ($t \geq 145$ μs) is gated out is shown Fig. 10a. As expected, the incident wave spectrum of the pristine plate and that of the plate with linear delamination are equal. The frequency spectrum of the reflected wavelet when the

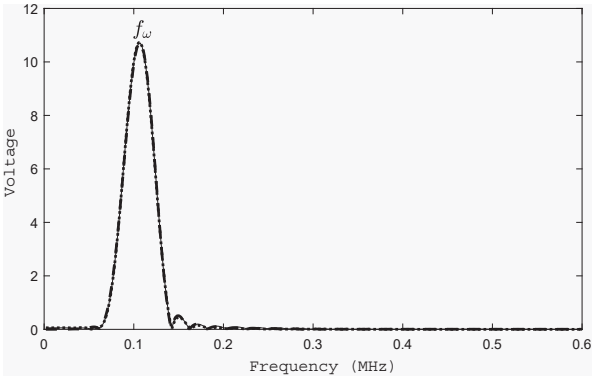

(a) Incident signal

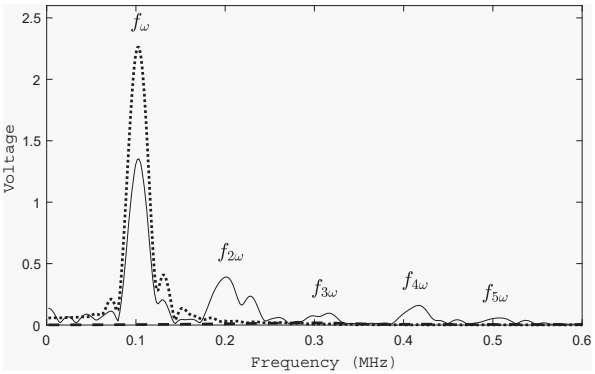

(b) Reflected signal

Fig. 10 Superimposed frequency spectral of the incident and the reflected wavelets: pristine plate (- -); plate with linear delamination ($\cdots$); plate with nonlinear delamination (-)

incident wavelet ($t \leq 145\ \mu s$) is gated out is shown in Fig. 10b. As observed, there exist spectrum component for only the fundamental harmonic. The absence of higher harmonics confirms the absence of nonlinearity in the plate with linear delamination.

4) Interaction with Nonlinear Delamination: Guided wave interaction with nonlinear delamination within the sandwich plate is considered in this section. Based on the developed scheme, the clapping delamination opens and closes under tension and compression respectively.

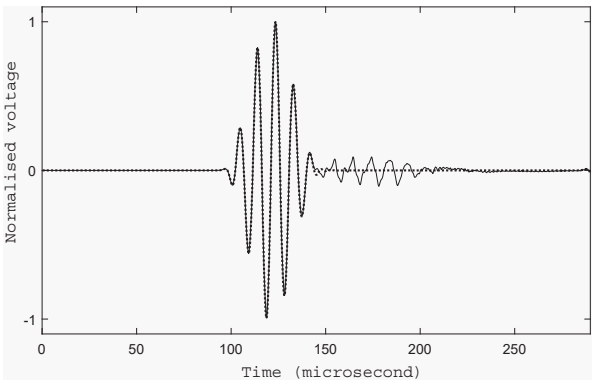

Fig. 11 Superimposed time history predictions for the pristine plate ($\cdots$) and the plate with nonlinear delamination (-)

The time history of the response obtained for the plate with nonlinear delamination at delamination width 0.3 of the plate thickness is presented in Fig. 11. It is superimposed with the time history of the response obtained for the pristine plate.

Similar to the response obtained for the plate with linear delamination, the response contains two wave packets; incident and reflected packets. But unlike the linear case, the reflected wave packet of the nonlinear case shows distortion along its path. This is due to contact acoustic nonlinearity within the nonlinear system. The presence of the distorted reflected wave package is an indication of not just a damage but a nonlinear damage in the structural waveguide.

The frequency spectrum of the incident wave package and that of the reflected wave package, when the reflected ($t \geq 145\ \mu s$) and incident ($t \leq 145\ \mu s$) wave packages are respectively gated out, are presented in Fig. 10 for the sandwich plate with nonlinear delamination. The results presented are superimposed with that of the pristine plate and the plate with linear delamination. As observed from the presented results, the frequency spectrum of the incident wave equals to those obtained for the pristine plate as well as the plate with linear delamination. It should be noted that the spectrum is purely linear, i.e. no generation of harmonics is observed. This is because the wave has not interacted with the nonlinear delamination at that stage. However, the frequency spectrum of the reflected wave generates harmonic components up to the fifth harmonics. The presence of harmonic components in the frequency spectrum is a significant indication of the presence of nonlinearity in the system. It should also be noted that the amplitude of the spectrum component at fundamental frequency is lower in the nonlinear case compared to the linear case. This is as a result energy leaking to higher harmonics in the nonlinear case.

The results of the harmonic wave reflection coefficients, generated for the guided wave interaction with nonlinear delamination in the sandwich plate, as a function of the delamination severity are presented in Fig. 12.

As expected, due to energy dissipation of the wave to generate higher harmonics, it is observed that the reflection coefficients reduces as the harmonic frequency increases. Reflection coefficient of about 0.19 is obtained at the fundamental harmonic, compared to 0.056, 0.019 and 0.012 obtained at the second, third and fourth harmonics respectively. In relation to the delamination width severity, the reflection coefficient follows a quarter-sinusoidal profile. In each case, the reflection coefficient increases with the delamination severity until delamination of an average width of 0.7 of the plate thickness where the reflection coefficient starts reducing against the delamination severity. The outcome of the wave reflection coefficient relationship with delamination severity could, in principle, be used as an indicator for early monitoring and detection of a delamination. This outcome could also be used to measure the span of a delamination.

VI. Concluding Remarks

A WFE-based computational scheme for analysing and quantifying wave interaction with nonlinear damage in composite structure is presented in this chapter. The scheme

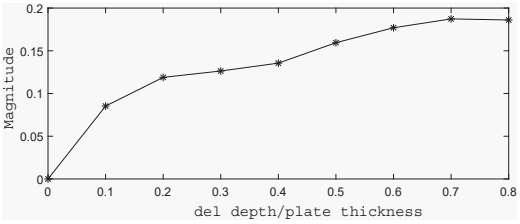

(a) 1st harmonic

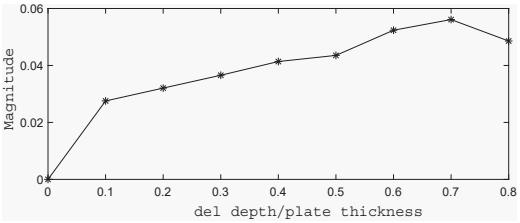

(b) 2nd harmonic

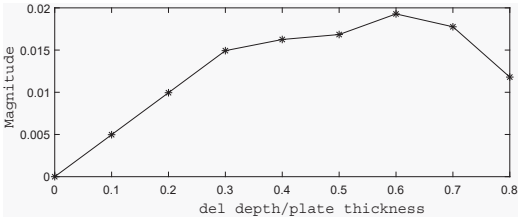

(c) 3rd harmonic

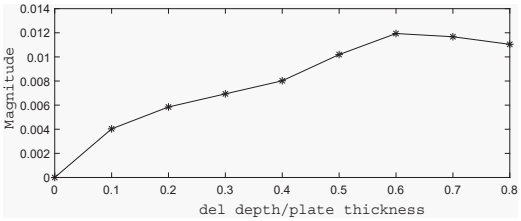

(d) 4th harmonic

Fig. 12 Wave interaction reflection coefficients for the sandwich plate with nonlinear delamination at different harmonic frequencies

can be applied to structures of arbitrary complexity, layering and material characteristics as an FE discretisation is employed. The scheme applies the WFE computed wave modes as time-dependent harmonic boundary conditions, using transient piezo-electrically generated ultrasonic wave, on the plate and is able to compute the generation of wave harmonics for each excited wave.

REFERENCES

[1] R. Soleimanpour and C.-T. Ng, "Locating delaminations in laminated composite beams using nonlinear guided waves," *Engineering Structures*, vol. 131, pp. 207–219, 2017.

[2] Y. Shen and V. Giurgiutiu, "Predictive modelling of nonlinear wave propagation for structural health monitoring with piezoelectric wafer active sensors," *Journal of Intelligent Material Systems and Structures*, vol. 25, pp. 506–520, 2014.

[3] X. Wan, Q. Zhang, G. Xu, and P. W. Tse, "Numerical simulation of nonlinear lamb waves used in a thin plate for detecting buried micro-cracks," *Sensors*, vol. 14, no. 5, pp. 8528–8546, 2014.

[4] B. R. Mace, D. Duhamel, M. J. Brennan, and L. Hinke, "Finite element prediction of wave motion in structural waveguides," *The Journal of the Acoustical Society of America*, vol. 117, no. 5, pp. 2835–2843, 2005.

[5] J. M. Mencik and M. N. Ichchou, "Multi-mode propagation and diffusion in structures through finite elements," *European Journal of Mechanics-A/Solids*, vol. 24, no. 5, pp. 877–898, 2005.

[6] V. Thierry, L. Brown, and D. Chronopoulos, "Multi-scale wave propagation modelling for two-dimensional periodic textile composites," *Composites Part B: Engineering*, vol. 150, pp. 144–156, 2018.

[7] T. Ampatzidis, R. K. Leach, C. Tuck, and D. Chronopoulos, "Band gap behaviour of optimal one-dimensional composite structures with an additive manufactured stiffener," *Composites Part B: Engineering*, vol. 153, pp. 26–35, 2018.

[8] D. Chronopoulos, "Design optimization of composite structures operating in acoustic environments," *Journal of Sound and Vibration*, vol. 355, pp. 322–344, 2015.

[9] S. Cantero-Chinchilla, J. Chiachío, M. Chiachío, D. Chronopoulos, and A. Jones, "A robust bayesian methodology for damage localization in plate-like structures using ultrasonic guided-waves," *Mechanical Systems and Signal Processing*, vol. 122, pp. 192–205, 2019.

[10] R. Apalowo and D. Chronopoulos, "A wave-based numerical scheme for damage detection and identification in two-dimensional composite structures," *Composite Structures*, vol. 214, pp. 164–182, 2019.

[11] D. Chronopoulos, "Wave steering effects in anisotropic composite structures: Direct calculation of the energy skew angle through a finite element scheme," *Ultrasonics*, vol. 73, pp. 43–48, 2017.

[12] R. Apalowo, D. Chronopoulos, and G. Tanner, "Wave interaction with defects in pressurised composite structures," *Journal of Nondestructive Evaluation*, vol. 37, no. 3, p. 48, 2018.

[13] R. Apalowo, D. Chronopoulos, M. Ichchou, Y. Essa, and F. Martin De La Escalera, "The impact of temperature on wave interaction with damage in composite structures," *Proceedings of the Institution of Mechanical Engineers, Part C: Journal of Mechanical Engineering Science*, vol. 231, no. 16, pp. 3042–3056, 2017.

[14] R. K. Apalowo, D. Chronopoulos, and M. Malik, "The influence of temperature on wave scattering of damaged segments within composite structures," in *MATEC Web of Conferences*, vol. 211. EDP Sciences, 2018, p. 19005.

[15] D. Chronopoulos, C. Droz, R. Apalowo, M. Ichchou, and W. Yan, "Accurate structural identification for layered composite structures, through a wave and finite element scheme," *Composite Structures*, vol. 182, pp. 566–578, 2017.

[16] I. ANSYS, *ANSYS 14.0 User's Help*, 2014.

[17] J. M. Renno and B. R. Mace, "Calculation of reflection and transmission coefficients of joints using a hybrid element/wave and finite element approach," *Journal of Sound and Vibration*, vol. 332, pp. 2149–2164, 2013.

[18] J. Nienwenhui, J. Neumann, D. Greve, and I. Oppenheim, "Generation and detection of guided waves using pzt wafer transducers," *IEEE transactions on ultrasonics, ferroelectrics, and frequency control*, vol. 52, no. 11, pp. 2103–2111, 2005.